Supplementary information

Copper (II) Infused Porphyrin MOF: Maximum Scavenging GSH for Enhanced Photodynamic Disruption of Bacterial Biofilm

Yaoxin Zhang,[a] Linpei Li,[a] Hui Liu,[c] Haixia Zhang,[a] Menghao Wei,[a] Junqing Zhang,[a,e] Yanwei Yang,[d] Mengnan Wu,[f] Zhaowei Chen,[f] Chaoqun Liu,*[a,d] Faming Wang,*[b] Qiang Wu,*[a] Jiahua Shi*[e]

[a] School of Pharmacy, Henan University, Kaifeng 475004, China.

[b] School of Public Health, Nantong Key Laboratory of Public Health and Medical Analysis, Nantong University, Nantong 226019, China

[c] Department of Pharmacy, Shangqiu First People's Hospital, Shangqiu 476100, China.

[d] Department of Pharmacy, the First Affiliated Hospital of Henan University, Kaifeng 475001, China.

[e] Key Laboratory of Natural Medicine and Immune-Engineering of Henan Province, Henan University, Kaifeng 475004, China.

[f] Institute of Food Safety and Environment Monitoring, College of Chemistry, Fuzhou University, Fuzhou 350108, China.

Corresponding Authors:

E-mail: cqliu@henu.edu.cn; wangfaming1990@ntu.edu.cn; henuwuqiang@henu.edu.cn; sjiahua@henu.edu.cn.

1.1 Materials

Zirconyl chloride octahydrate ($ZrClO_2 \cdot 8H_2O$), Tetrakis (4-carboxyphenyl) porphyrin (TCPP), and benzoic acid (BA) were obtained from Aladdin Chemistry (Shanghai, China). Fluorescent diacetate (FDA) and propidium iodide (PI) were purchased from Solarbio (Beijing, China). Nutrient agar, trypticase soy broth (TSB) and dulbecco's modified eagle medium (DMEM) were obtained from Aoboxing Biotechnology (Beijing, China). $CuCl_2 \cdot 2H_2O$, Reduced glutathione (GSH), and 5,5′-dithiobis (2-nitrobenzoic acid) (DTNB) was purchased from Aladdin Chemistry (Shanghai, China). Reactive oxygen species detection probe (DCFH-DA) was purchased from Beyotime Biotechnology. Staphylococcus aureus (*S. aureus*) (ATCC 25923) and Escherichia coli (*E. coli*) (ATCC 25922) strains were provided by Chuanxiang Biotechnology (Shanghai, China).

1.2 Instrumentation

Scanning electron microscopy (SEM) images were acquired with a Hitachi S-4800 FESEM. Transmission electronic microscope (TEM) images and elemental mappings were acquired with a TEM system (FEI Tecnai G2 F20) with an accelerating voltage of 100 keV. N_2 adsorption-desorption isotherms were acquired with a Micromeritics ASAP 2020M automated sorption analyzer. Dynamic light scattering and Zeta potential were obtained by a Malvern Zetasizer Nano ZS90. X-ray diffraction (XRD) analysis was carried out by using a Bruker D8 Advance diffractometer with Cu Kα radiation. Fourier transform infrared (FTIR) spectra was recorded on a Bruker Vertex 70 spectrometer. The UV-Vis spectra were obtained from a Shimadzu UV-2600 UV-Vis spectrophotometer. X-ray photoelectron Spectroscopy (XPS) spectra was analyzed with a VG Scientific ESCALab220i-XL electron spectrometer. Fluorescence images were captured on an Olympus BX-51 fluorescence microscope. ICP-MS measurements were performed using a Thermo Fisher Scientific X SERIES2 ICP-MS. *In vivo* fluorescence imaging system were captured on an IVIS Lumina XRMS Series.

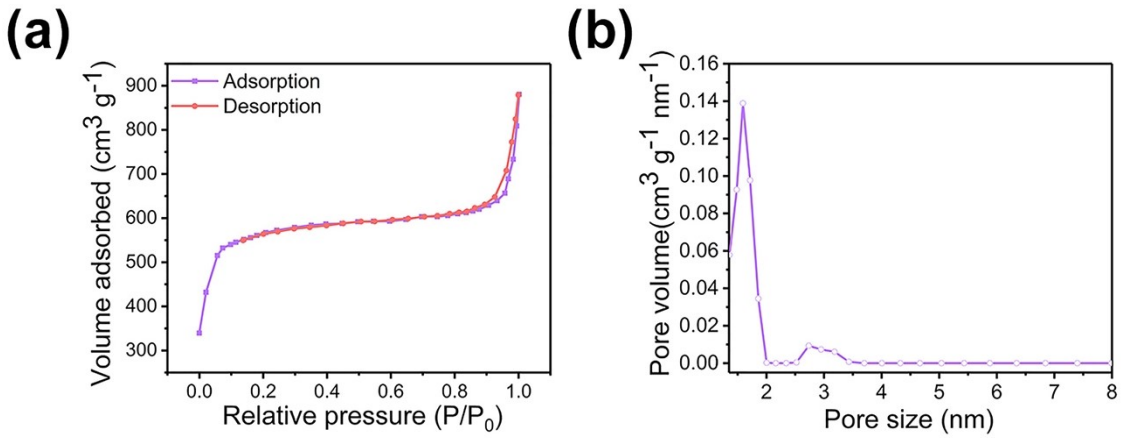

Fig. S1 (a) Nitrogen sorption-desorption isotherms of MOF and (b) pore size distribution profile of MOF.

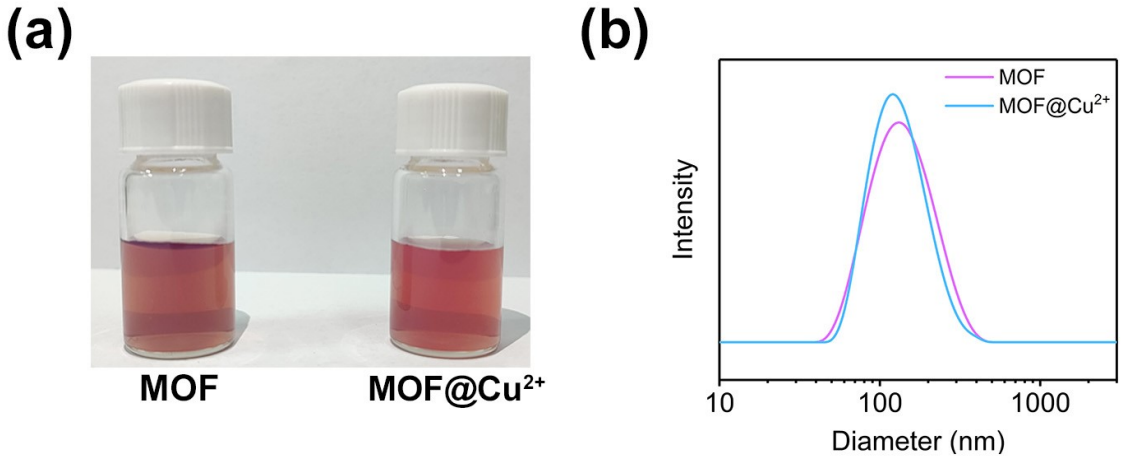

Fig. S2 (a) Water dispersibility of MOF and MOF@Cu^{2+}. (b) Size distribution of MOF and MOF@Cu^{2+}.

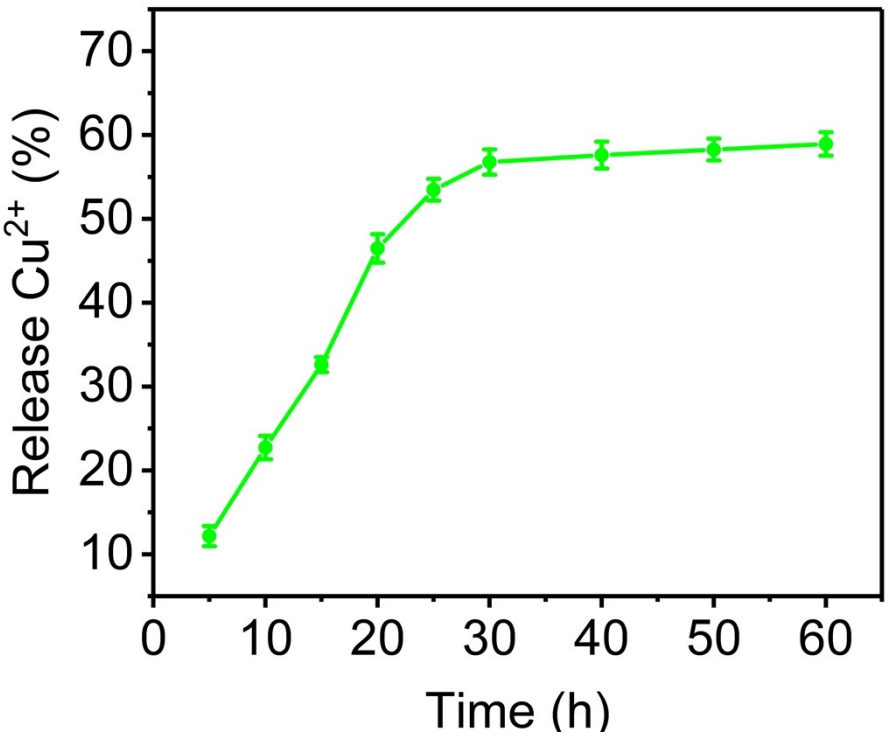

Fig. S3 Cu^{2+} release profile of MOF@Cu^{2+} immersed in deionized water for 60 h. (n = 3; mean ± SD)

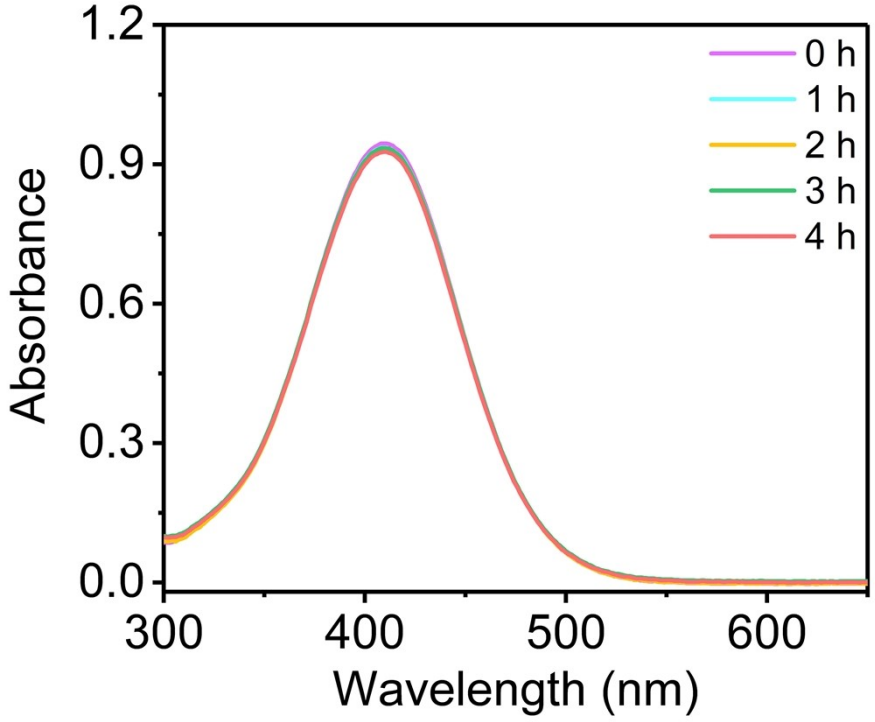

Fig. S4 UV-vis spectra of DTNB solution after incubating with MOF for different time.

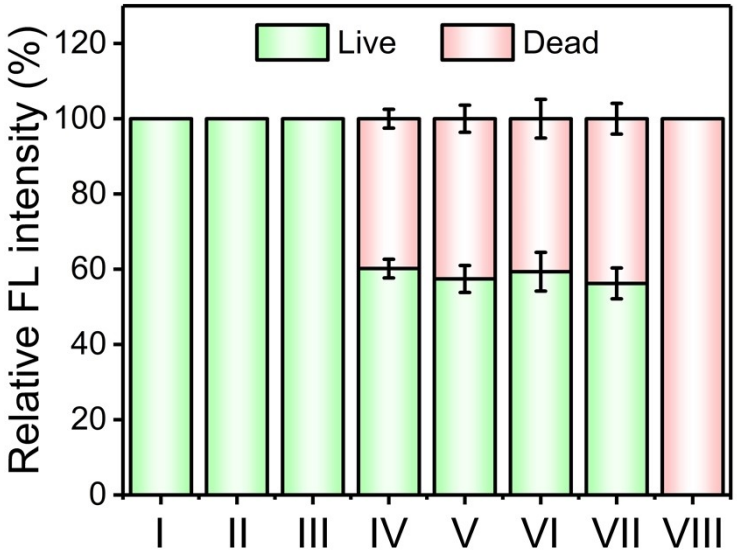

Fig. S5 The semi-quantitative statistics of live/dead fluorescence intensity and of *S. aureus*. ((I) saline, (II) saline + L, (III) MOF, (IV) MOF + L, (V) Cu^{2+}, (VI) Cu^{2+} + L, (VII) MOF@Cu^{2+}, (VIII) MOF@Cu^{2+} + L (n = 3; mean ± SD).

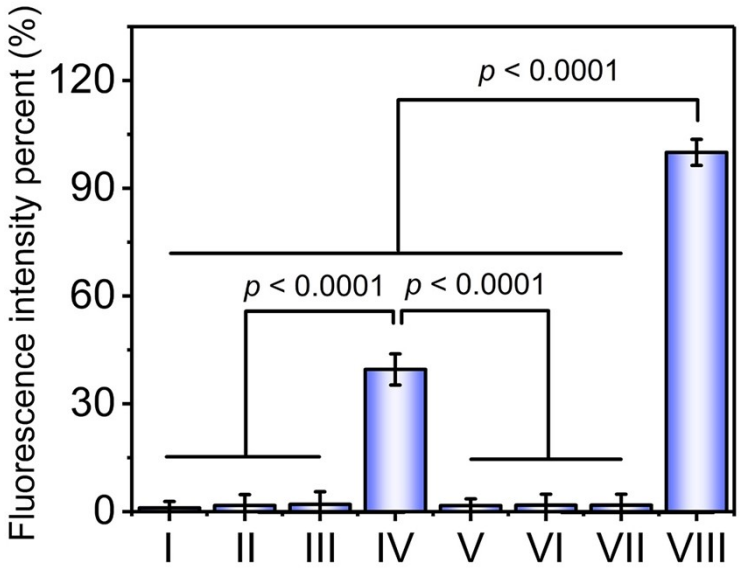

Fig. S6 The semi-quantitative statistics of ROS fluorescence intensity of *S. aureus*. ((I) saline, (II) saline + L, (III) MOF, (IV) MOF + L, (V) Cu^{2+}, (VI) Cu^{2+} + L, (VII) MOF@Cu^{2+}, (VIII) MOF@Cu^{2+} + L (n = 3; mean ± SD). Statistical significance was calculated by one-way ANOVA using the Tukey post-test.

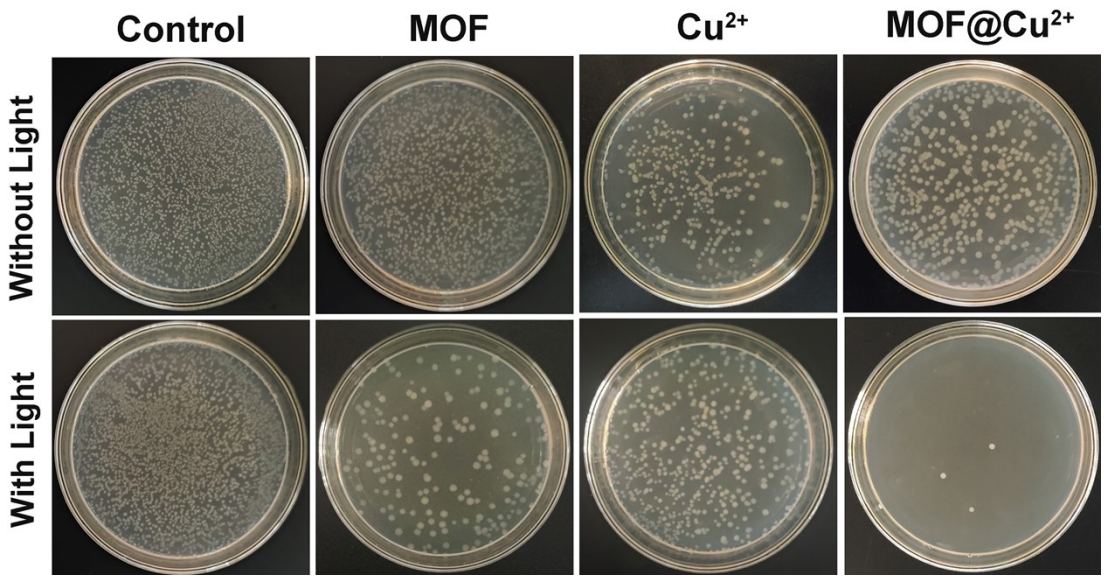

Fig. S7 Images of agar plates of *E. coli* after various therapies.

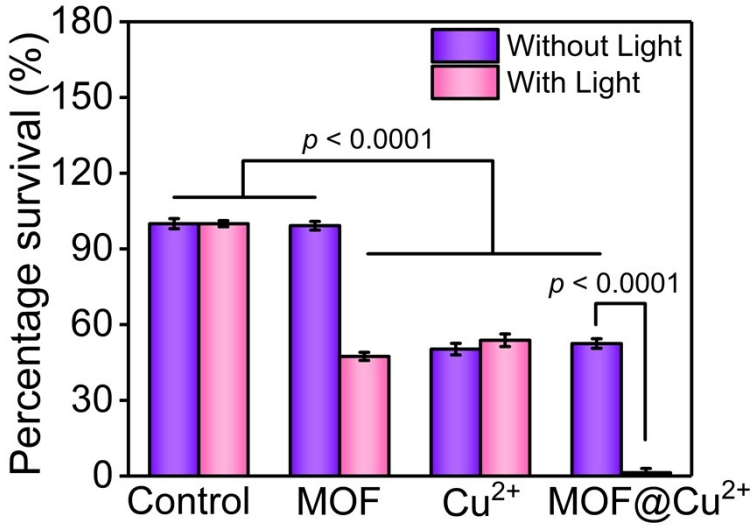

Fig. S8 Percentage survival rates obtained via counting *E. coli* colonies of Fig. S5 (n = 3; mean ± SD). Statistical significance was calculated by two-way ANOVA using the Tukey post-test.

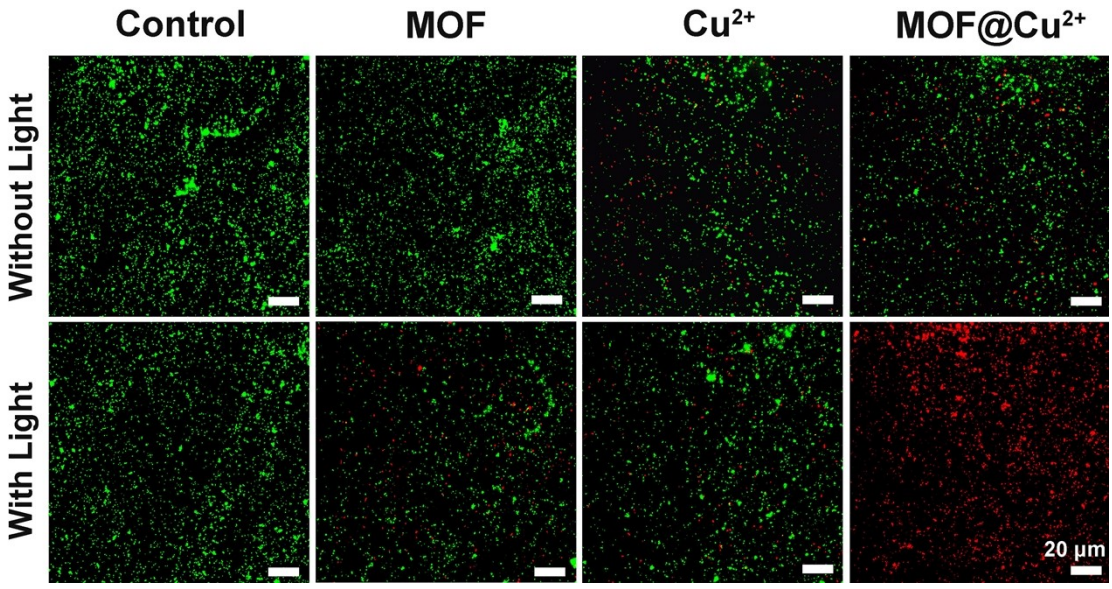

Fig. S9 Live/dead fluorescence images of *E. coli* stained by FDA (green, viable bacteria) and PI (red, dead bacteria) after different therapies.

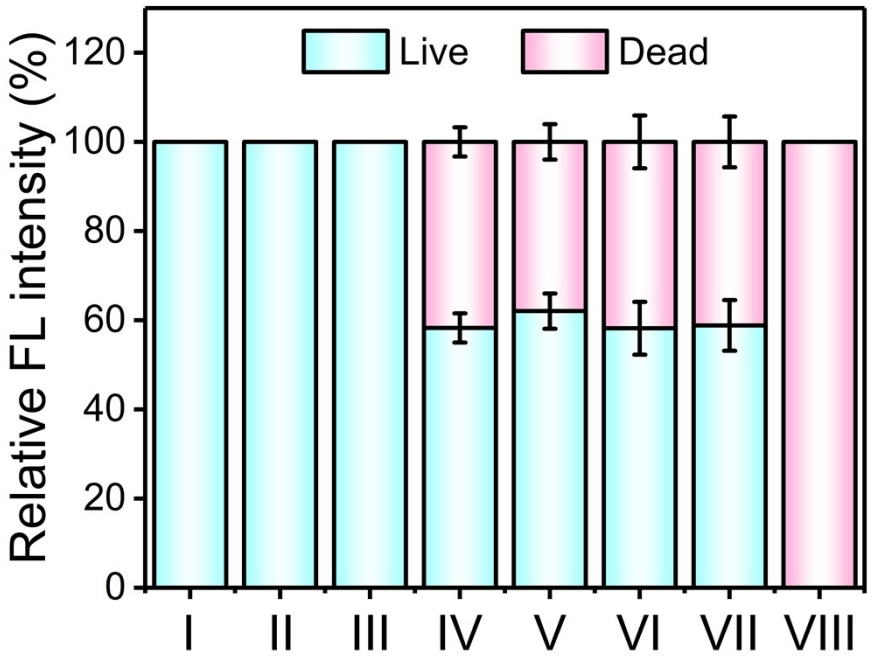

Fig. S10 The semi-quantitative statistics of live/dead fluorescence intensity and of *E. coli* ((I) saline, (II) saline + L, (III) MOF, (IV) MOF + L, (V) Cu^{2+}, (VI) Cu^{2+} + L, (VII) MOF@Cu^{2+}, (VIII) MOF@Cu^{2+} + L (n = 3; mean ± SD)).

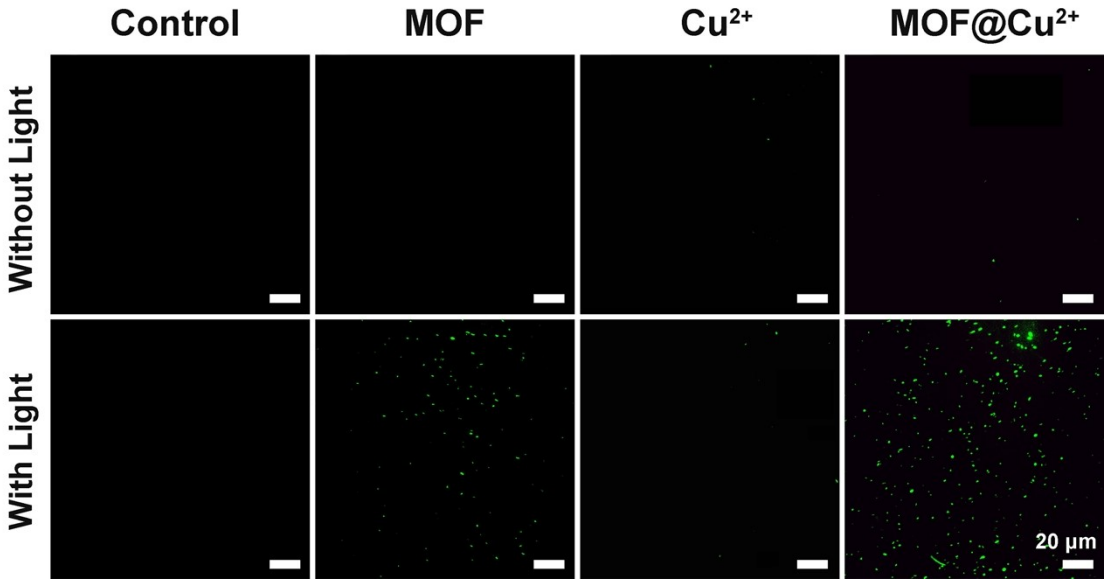

Fig. S11 Intracellular ROS fluorescent images of *E. coli* stained by DCFH-DA.

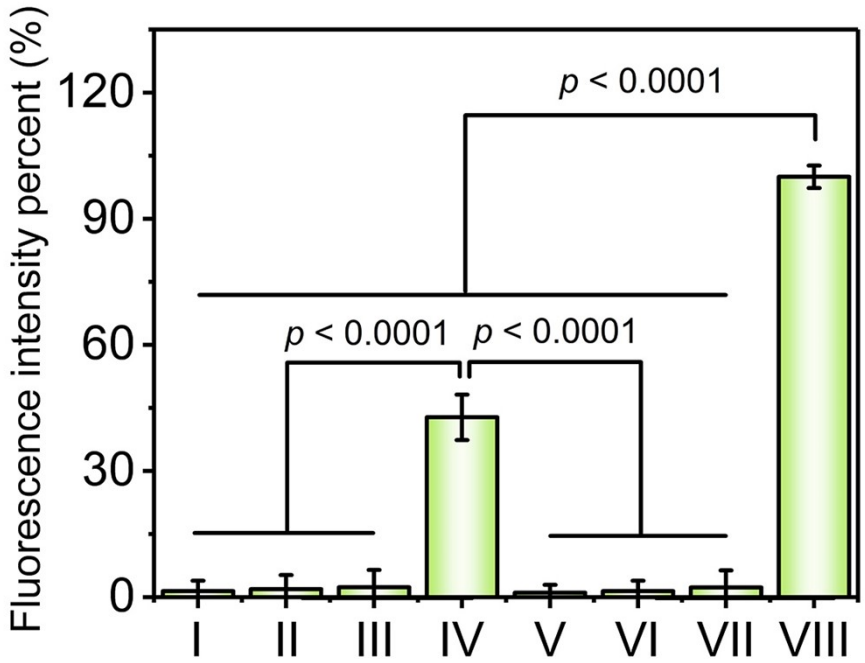

Fig. S12 The semi-quantitative statistics of ROS fluorescence intensity of *E. coli* ((I) saline, (II) saline + L, (III) MOF, (IV) MOF + L, (V) Cu^{2+}, (VI) Cu^{2+} + L, (VII) MOF@Cu^{2+}, (VIII) MOF@Cu^{2+} + L (n = 3; mean ± SD)). Statistical significance was calculated by one-way ANOVA using the Tukey post-test.

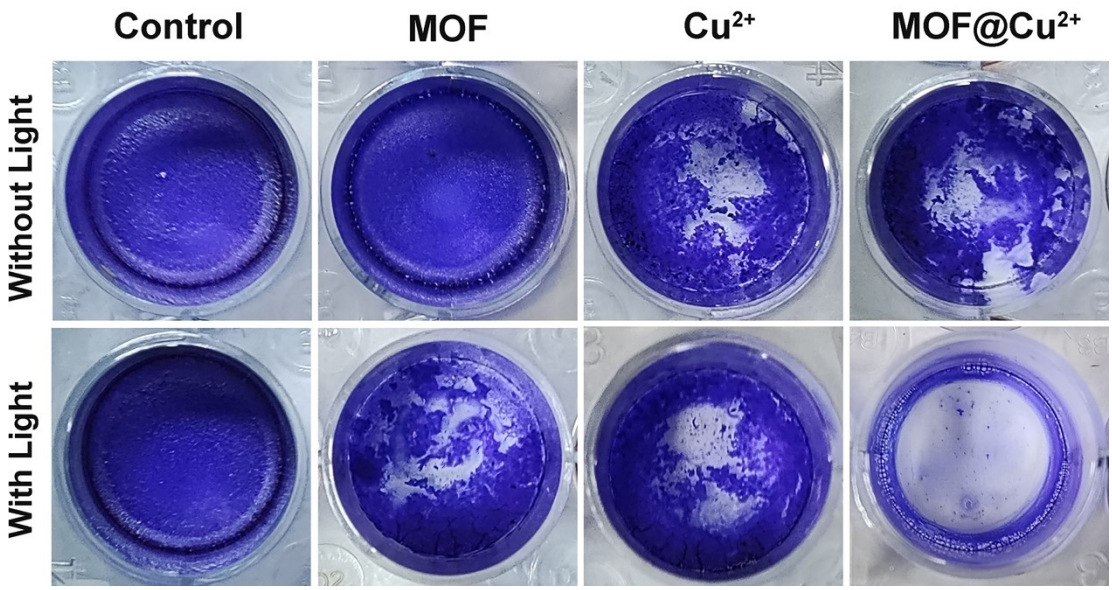

Fig. S13 Images of crystal violet-dyed *E. coli* biofilm after treating with various groups.

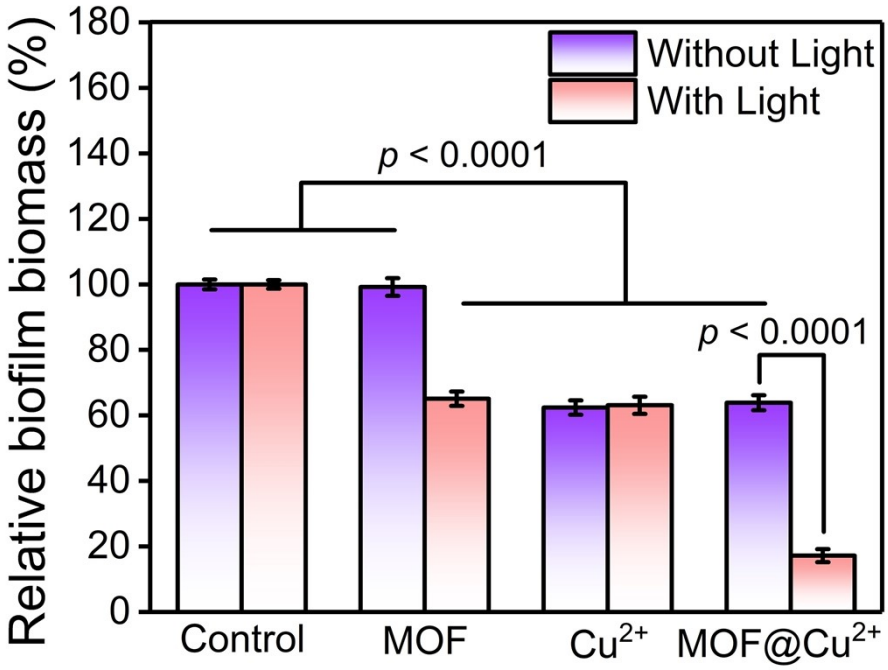

Fig. S14 Biomass of *E. coli* biofilm after treating with various groups (n = 3; mean ± SD). Statistical significance was calculated by two-way ANOVA using the Tukey post-test.

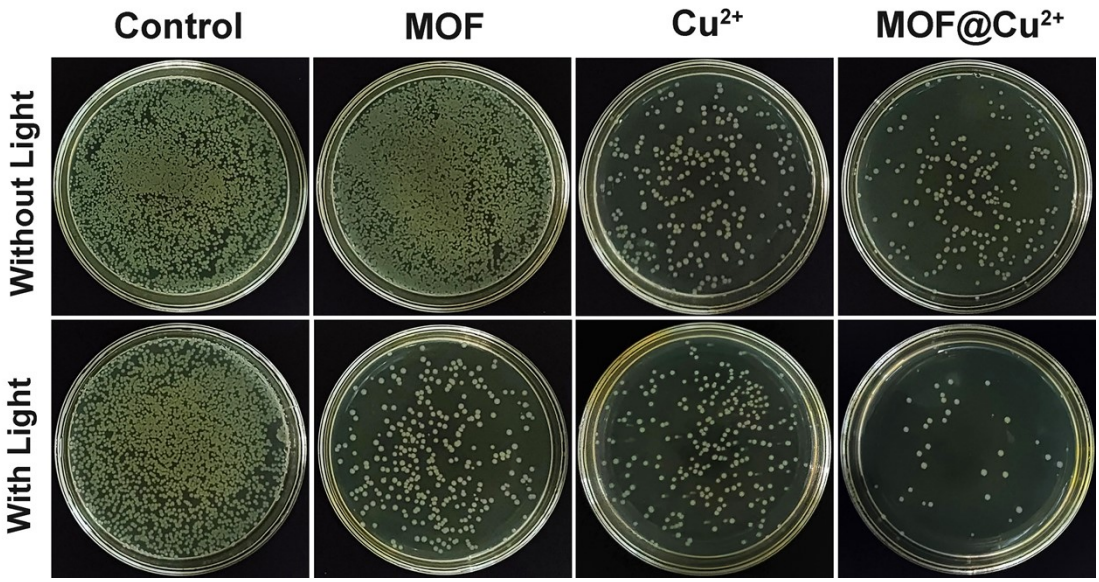

Fig. S15 Agar plates photographs of *E. coli* isolated from biofilm after various therapies.

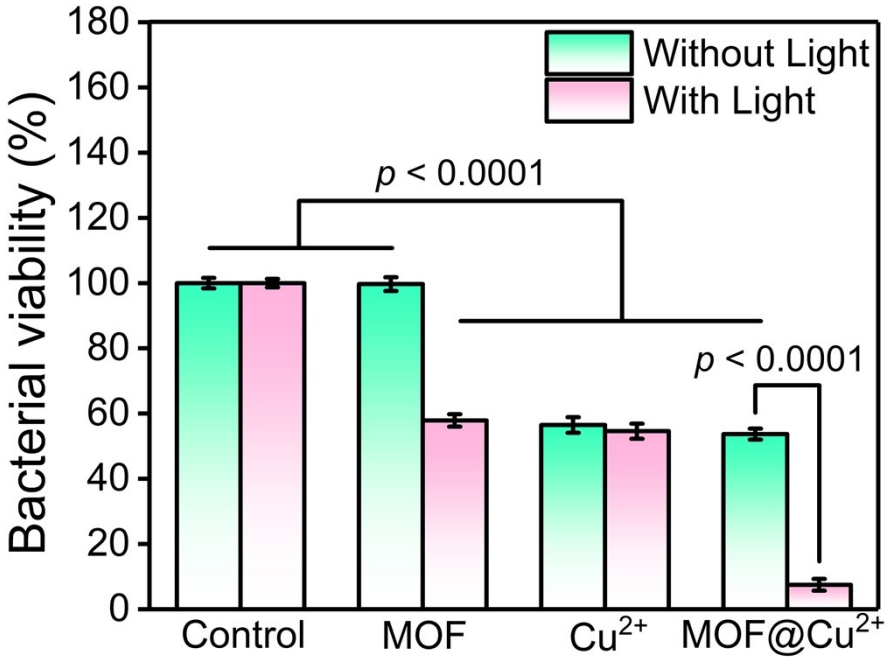

Fig. S16 Percentage survival rates of *E. coli* obtained from biofilm with various therapies (n = 3; mean ± SD). Statistical significance was calculated by two-way ANOVA using the Tukey post-test.

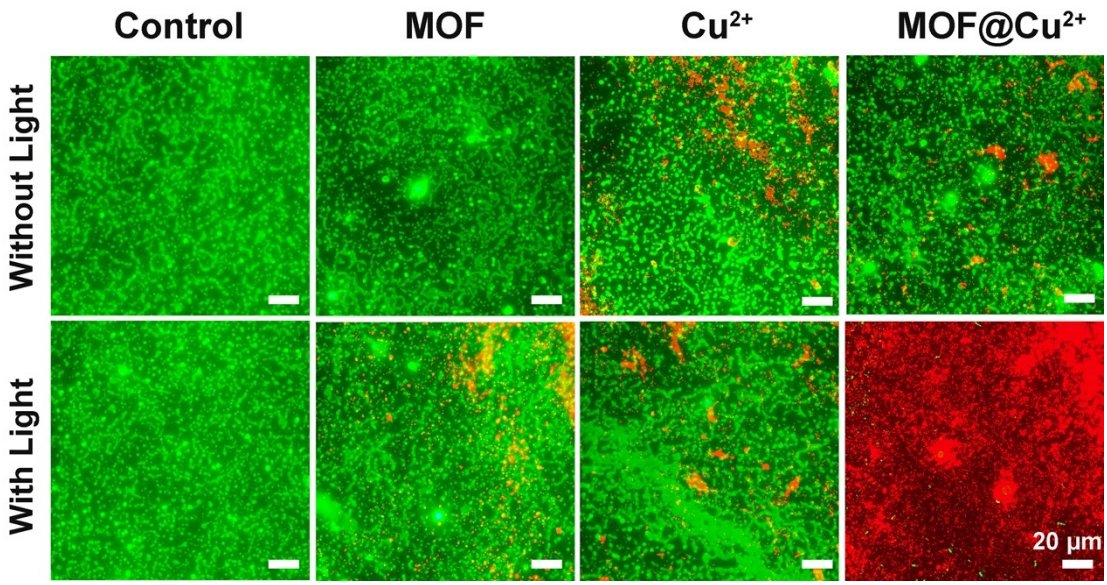

Fig. S17 Fluorescence images of *E. coli* biofilm after various therapies.

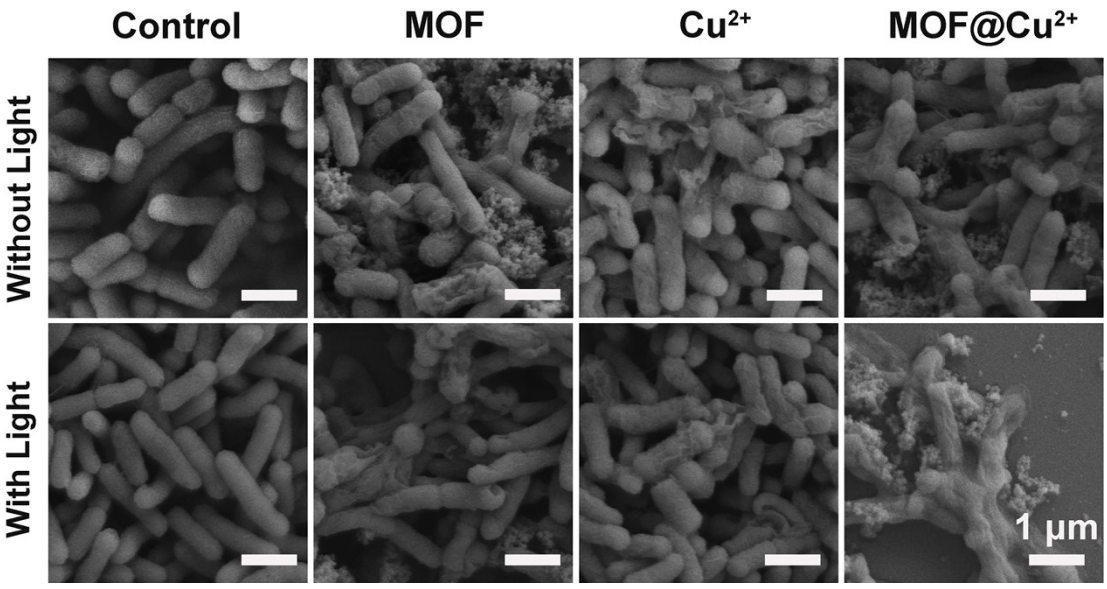

Fig. S18 SEM images of *E. coli* biofilm after various therapies.

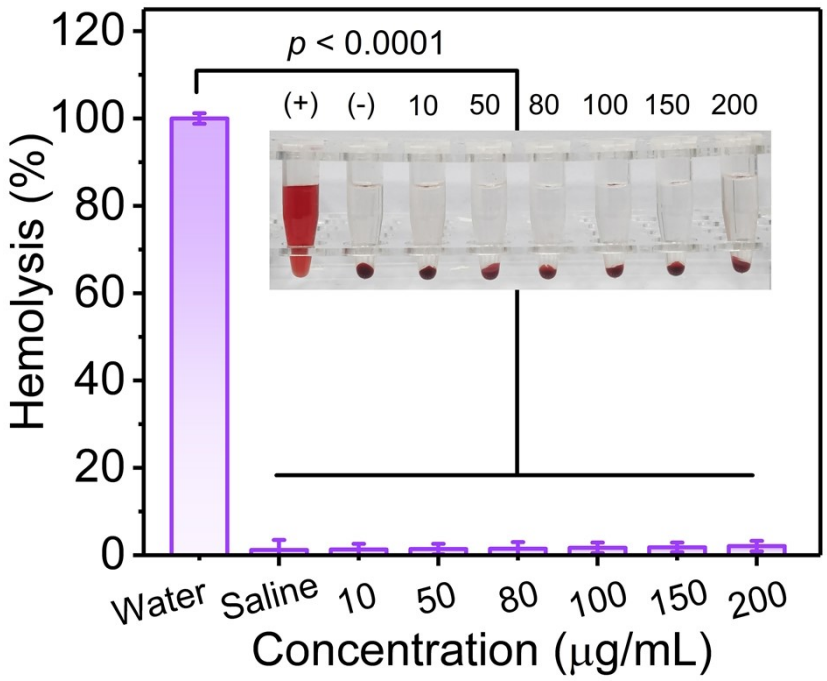

Fig. S19 Hemolysis activity assess of MOF@Cu^{2+} (n = 3; mean ± SD). Statistical significance was calculated by one-way ANOVA using the Tukey post-test.

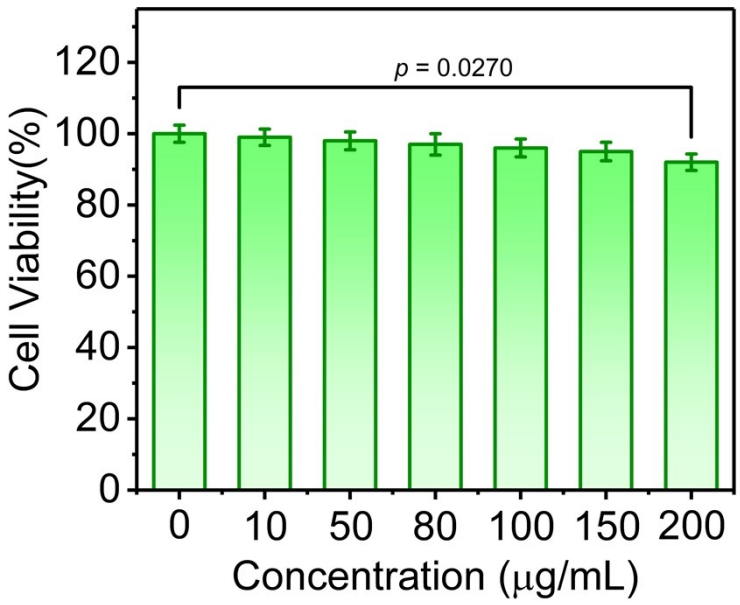

Fig. S20 *In vitro* cytotoxicity of L929 fibroblast cells after incubating with different concentrations of MOF@Cu^{2+} (n = 3; mean ± SD). Statistical significance was calculated by one-way ANOVA using the Tukey post-test.

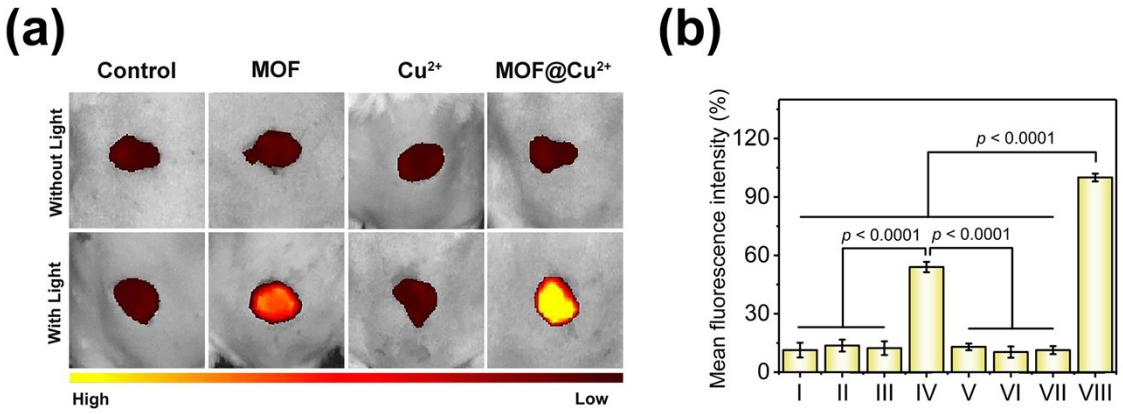

Fig. S21 (a) ROS fluorescence images of mice wounds before/after various treatments. (b) The quantitatively analysis of mean fluorescence intensities of ROS before/after various treatments ((I) saline, (II) saline + L, (III) MOF, (IV) MOF + L, (V) Cu^{2+}, (VI) Cu^{2+} + L, (VII) MOF@Cu^{2+}, (VIII) MOF@Cu^{2+} + L (n = 3; mean ± SD)). Statistical significance was calculated by one-way ANOVA using the Tukey post-test.

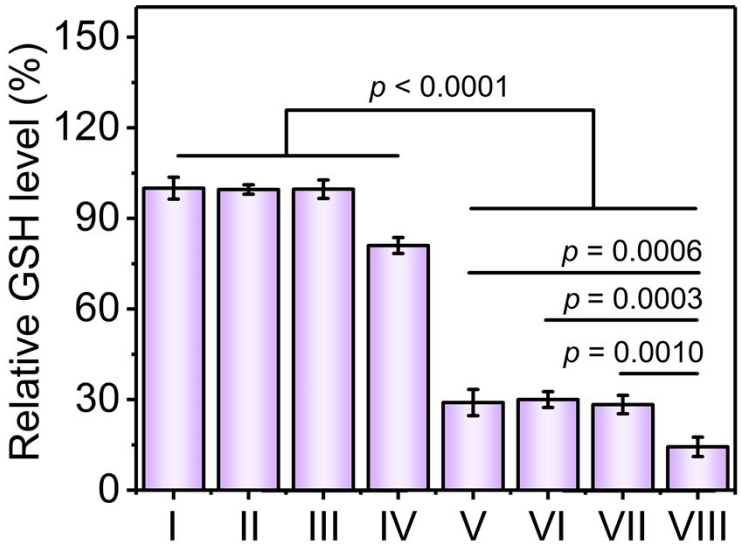

Fig. S22 GSH levels of mice wounds before/after various treatments ((I) saline, (II) saline + L, (III) MOF, (IV) MOF + L, (V) Cu^{2+}, (VI) Cu^{2+} + L, (VII) MOF@Cu^{2+}, (VIII) MOF@Cu^{2+} + L (n = 3; mean ± SD)). Statistical significance was calculated by one-way ANOVA using the Tukey post-test.

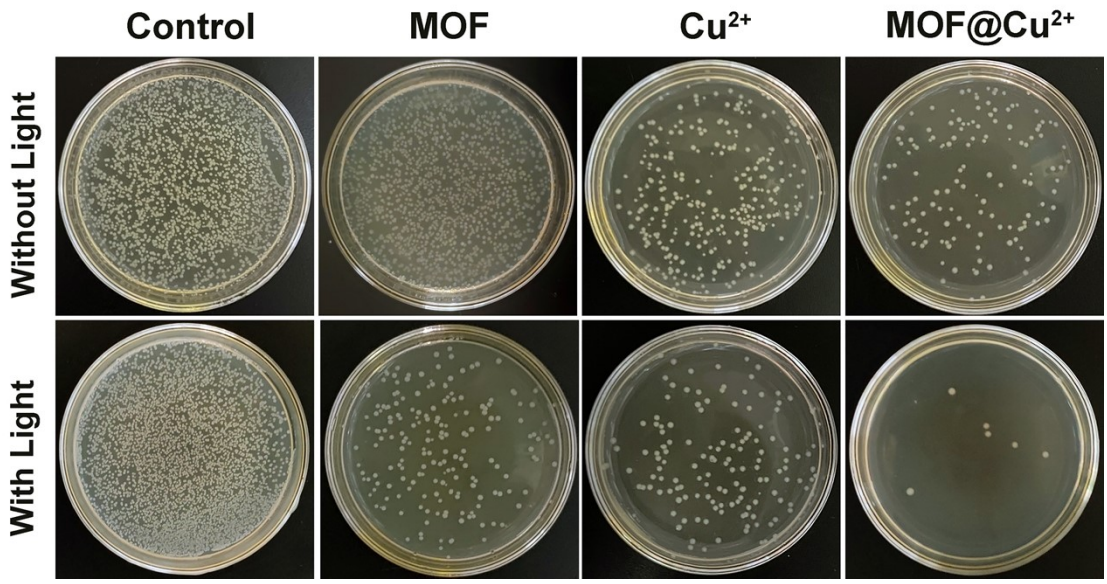

Fig. S23 Images of bacterial colonies obtained from wound tissues after various therapies.

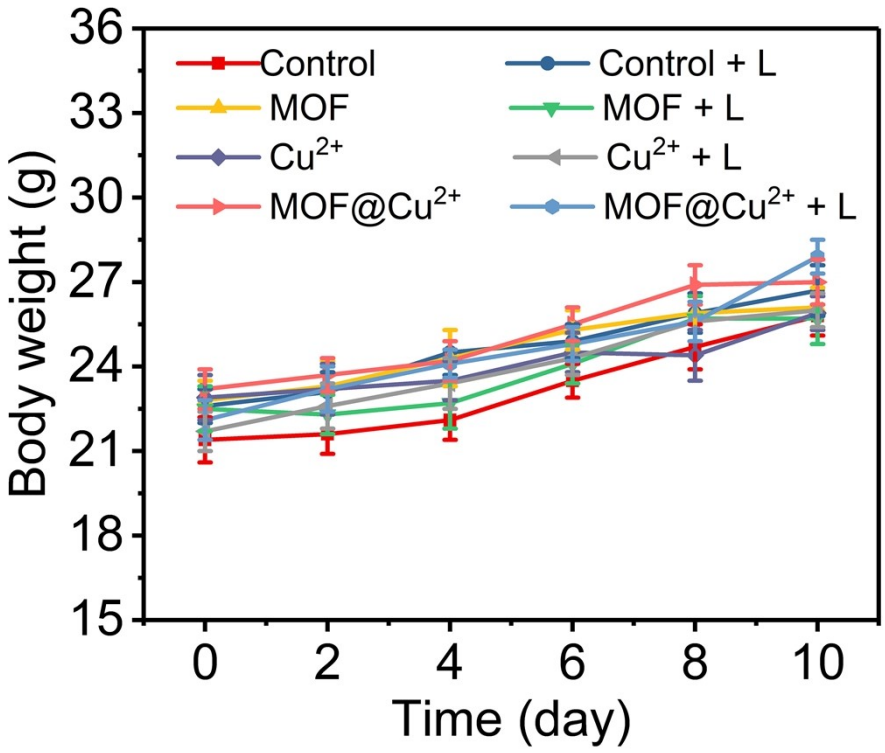

Fig. S24 Body weight changes of mice in various treatment groups. (n = 5; mean ± SD)

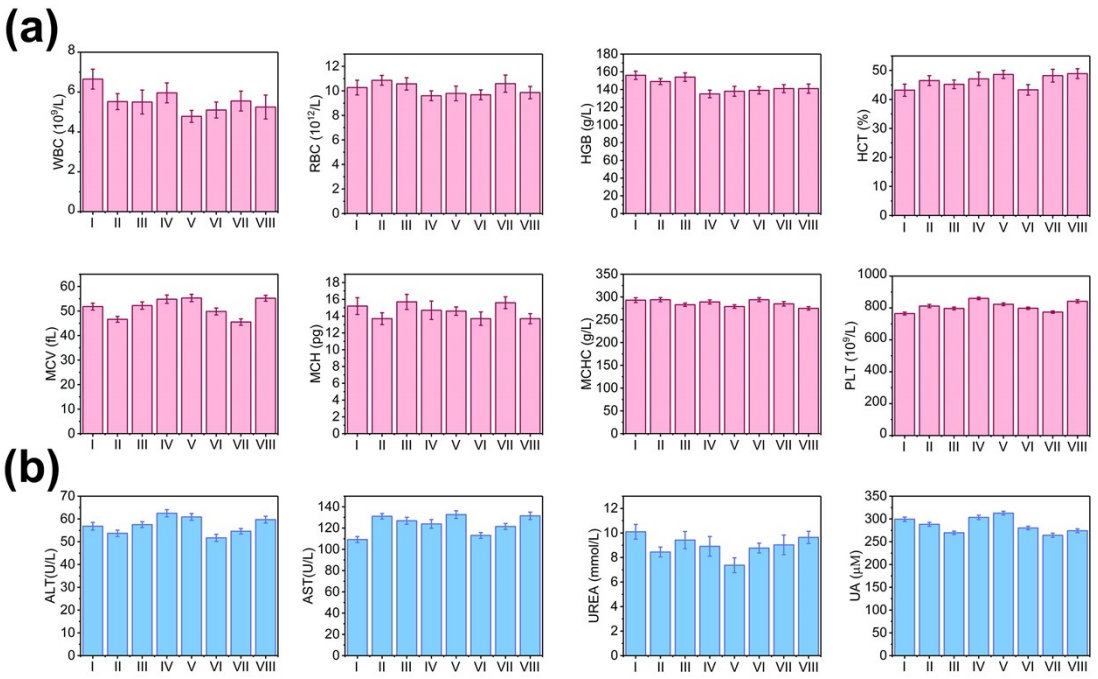

Fig. S25 (a) Levels of hematology examination indexes after various therapies. (b) Levels of blood biochemistry indexes of liver and kidney after various therapies. ((I) saline, (II) saline + L, (III) MOF, (IV) MOF + L, (V) Cu^{2+}, (VI) Cu^{2+} + L, (VII) MOF@Cu^{2+}, (VIII) MOF@Cu^{2+} + L (n = 3; mean ± SD)).